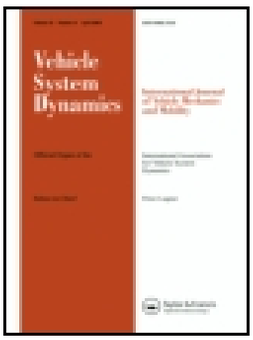

Vehicle System Dynamics

ISSN: 0042-3114 (Print) 1744-5159 (Online) Journal homepage: http://www.tandfonline.com/loi/nvsd20

Analysis of Automatic Steering Control for Highway Vehicles with Look-down Lateral Reference Systems

JÜRGEN GULDNER , HAN-SHUE TAN & SATYAJIT PATWARDHAN

To cite this article: JÜRGEN GULDNER , HAN-SHUE TAN & SATYAJIT PATWARDHAN (1996) Analysis of Automatic Steering Control for Highway Vehicles with Look-down Lateral Reference Systems, Vehicle System Dynamics, 26:4, 243-269, DOI: 10.1080/00423119608969311

To link to this article: https://doi.org/10.1080/00423119608969311

Published online: 27 Jul 2007.

Vehicle System Dynamics, 26 (1996), pp. 243–269 0042-3114/96/2604-2431$12.00

Analysis of Automatic Steering Control for Highway Vehicles with Look-down Lateral Reference Systems

JÜRGEN GULDNER*, HAN-SHUE TAN* and SATYAJIT PATWARDHAN*

SUMMARY

In this paper, steering control for passenger cars on automated highways is analyzed, concentrating on look-down reference systems. Extension of earlier experimental results for low speed to highway speed is shown to be non-trivial. The limitations of pure output-feedback of lateral vehicle displacement from the road reference are examined under practical constraints and performance requirements like robustness, maximum lateral error and comfort. The in-depth system analysis directly leads to a new alternative design direction which allows to preserve look-ahead reference systems for highway speed automatic driving.

1. INTRODUCTION

Automatic steering control is a vital component of highway automation, currently investigated worldwide in several programs, e.g. ITS in the US and PVS, SSVS and ARTS under ITS Japan. Overviews of highway automation were given, for example, by Bender [1] and Shladover [2]; a possible scenario was outlined by Varaiya [3]. The steering control task, at first sight, appears straight-forward: Design a controller which steers a road vehicle along a given reference path on the road. Millions of human drivers perform this task quite well every day. In experimental implementation, however, control design for highway driving encounters significant challenges of practical and technological nature. The main obstacles relate to sensing the lateral displacement, performance and robustness requirements, and steering actuation.

Human drivers use visual perception for lane keeping control. This "technique" has been replicated with several vision-based automatic steering approaches. In order to remedy the susceptibility of vision systems to road and weather conditions, alternative reference systems have been investigated. Examples are electric wire guidelines, first tested at The Ohio State University (OSU) in the US [4] for passenger cars and later by Daimler-Benz and MAN in Germany for buses [5]; radar reflecting guard rails studied at OSU [6]; and magnetic markers used in the California PATH project [7]. These approaches are all "look-down" systems,

* California PATH, University of California at Berkeley, Institute of Transportation Studies, 1357 S. 46th Street, Richmond, CA 94804-4698, USA. Tel. (510) 231 9494.

measuring the lateral displacement of the vehicle with respect to the road reference within the vehicle boundaries. In contrast to this, vision-based driving (human vision or machine vision) uses "look-ahead" information by measuring the lateral displacement, and often also angular displacement, at a large distance ahead of the vehicle outside the vehicle boundaries, possibly increasing the look-ahead distance with increasing velocity like human behavior. A similar effect can be achieved using radar reflective stripes [8] or other energy emitting or reflecting devices [9].

Human driving performance readily adapts to traffic situations. In heavy traffic and on narrow lanes, e.g. near construction sites, we concentrate on lane keeping with small errors. On wide, open highways, however, concentration decreases and so does the tracking performance. While the width of passenger cars including side-mirrors varies within 6 to 8 ft (approx. 1.8–2.4 m) from subcompacts to full-size vans and pick-ups, US highway lanes have a width of 12 ft (approx. 3.6 m), leaving a worst-case margin of 2 ft (approx. 60 cm) on each side for lane keeping errors. An automatic steering system is expected to achieve tight tracking performance [10], e.g. a maximum error of $\frac{1}{2}$ ft (approx. 15 cm) under normal conditions and below 1 ft (approx. 30 cm) in extreme situations. Such specifications would allow an additional 1 ft (approx. 30 cm) safety margin for emergency situations like tire bursts [11].

Along with the performance requirements, ride comfort specifications such as good damping at all relevant frequencies and low lateral acceleration generated by the controller have to be satisfied. Furthermore, noise both in the reference itself and in sensor measurements has to be taken into account for controller design.

Performance and ride comfort requirements have to be satisfied under a wide range of operating conditions. While some slowly time-varying system parameters can be estimated and henceforth adapted for (e.g. car mass and inertia), road conditions may change abruptly, especially the road/tire adhesion factor. An automatic steering controller is required to be robust against such abrupt changes, e.g. water puddles ("hydro-planing") or ice pads. Consequently, the automatic steering control loop has to be simultaneously stable for all plausible road conditions, though with relaxed performance requirements for extreme situations. Parameter estimation and adaptation cannot be relied upon for sudden transitions, making robust steering control design indispensable.

The last issue of practical relevance discussed here is the steering actuator. Cost and power considerations impose bandwidth limitations of at most 10 Hz on a position-controlled, third or higher order steering actuator, regardless whether it is electric or hydraulic. Since the actuator bandwidth is subject to uncertainty with respect to operating conditions like temperature and command amplitude, a worst-case bandwidth of 5 Hz proved realistic in the experiments performed at California PATH. Compared with a human driver (below 1 Hz) and the car dynamics (up to 2 Hz), this constitutes a serious factor, considering the discussed performance, comfort and robustness requirements. Unlike in many classical control problems, the actuator dynamics are an inherent system component and need to be considered during control design.

From a control point of view, four wheel steering (4WS) is an attractive alternative which would provide two independent control inputs. Cost factors, however, reduce the practicality of 4WS for wide-spread application and lead us to concentrate on front-wheel-steered cars.

A large body of literature is available for steering control of automated guided vehicles (AGVs). Unfortunately, those results cannot be easily transferred to road vehicles and highway driving since the main control issue for AGVs are the, often nonholonomic kinematics, rather than the dynamics as for road vehicles.

For road vehicles, look-down systems have been successfully implemented and demonstrated by several research groups, including Daimler-Benz/MAN [5], OSU [12], PATH [13] and, most recently, in Japan [14]. However, the experimental results were all obtained below highway speed. The uniform limitation of driving speed to maximally 40 mph (approx. 65 km/h) in all experiments known to the authors is, in fact, disturbing. Furthermore, the requirements outlined above (performance, robustness and actuation) could not be met simultaneously in most experimentally verified approaches. Notable exceptions are the experiments performed at OSU in the 70ies [4], achieving up to 80 mph (approx. 128 km/h) under idealized conditions.

This paper analyzes the fundamental issues of automatic steering control for cars, concentrating on look-down systems at highway speed under practical conditions. The term "car" specifies a standard passenger car and is used interchangeably with the word "vehicle". Rather than designing yet another automatic steering controller, an in-depth system analysis is presented, leading to the conclusion that pure output feedback of lateral displacement at the front bumper is impractical for highway speed driving. The system analysis also leads to an intuitive future design direction.

After defining the lateral control design problem in Section 2, we present a detailed system analysis in Section 3. Section 4 examines pure output feedback of lateral displacement for low and high speed. Alternative controller structures are discussed in Section 5. We conclude in Section 6 that the automatic steering control problem has been underestimated for the case of highway driving under practical constraints and suggest future design directions.

2. PROBLEM STATEMENT

In this section, we present a detailed description of the automatic steering control problem. In addition to the mathematical model used for the system analysis in the subsequent sections, practical design constraints and performance requirements are discussed.

Task: Automatic Steering Control

Given a reference path and a road vehicle equipped with sensor(s) to detect lateral displacement from the reference and with an actuator to generate a

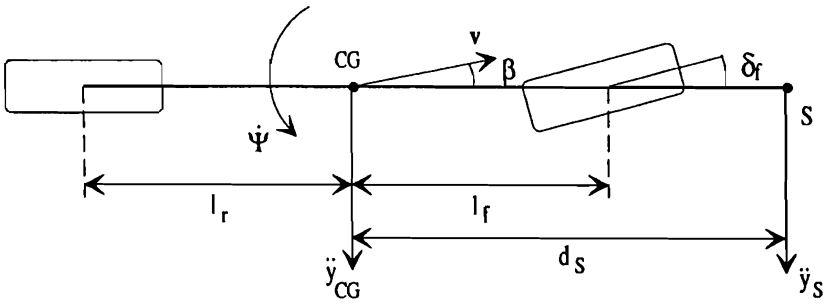

Fig. 1. Single-track model for car steering.

desired steering action, derive a controller for following the reference path under the performance, robustness and ride comfort requirements, and within the practical constraints described below.

The road reference can be continuous or discrete. Sensor(s) measure the distance of the vehicle from the reference path (lateral displacement) at some distance d_S in front of the vehicle's center of gravity (CG). For look-down systems, the sensor is located within the vehicle boundaries, usually at the front bumper. Kinematic and dynamic car models are presented in Section 2.1 and the controller specifications are summarized in Section 2.2.

2.1. Model for Automatic Steering Control

A linearized model has proved sufficient for studying car steering under "normal" conditions, i.e. non-emergency situations [15]. Assuming small angles, this allows to use the classical single-track model of Riekert-Schunk [16] shown in Fig. 1, also refered to as the "bicycle model". The two front wheels and the two rear wheels are respectively combined into a single wheel at front and back. A linear tire model is used under the assumption of small angles during "normal" highway driving conditions within the physical limits of tires. The variables denote:

- $\mathbf{v}$ vehicle velocity vector with $v = |\mathbf{v}| > 0$ (magnitude v is assumed measurable)
- β side-slip angle between vehicle longitudinal axis and velocity vector $\mathbf{v}$ at CG
- Ψ vehicle yaw angle with respect to a fixed inertial coordinate system
- $\dot{\Psi}$ vehicle yaw rate with respect to a fixed inertial coordinate system
- $\ddot{y}_{CG}$ lateral acceleration at CG with respect to a fixed inertial coordinate system
- $\ddot{y}_S$ lateral acceleration at location S with respect to a fixed inertial coordinate system
- δ_f front wheel steering angle

The linearized state-space model can be found e.g. in [15,17] as

$$\frac{d}{dt}\begin{bmatrix}\beta\\ \dot{\Psi}\end{bmatrix}=\begin{bmatrix}-\dfrac{\mu(c_f+c_r)}{Mv} & -1+\dfrac{\mu(c_r\ell_r-c_f\ell_f)}{Mv^2}\\ -\dfrac{\mu(c_r\ell_r-c_f\ell_f)}{I_\Psi} & -\dfrac{\mu(c_f\ell_f^2+c_r\ell_r^2)}{I_\Psi v}\end{bmatrix}\begin{bmatrix}\beta\\ \dot{\Psi}\end{bmatrix}+\begin{bmatrix}\dfrac{\mu c_f}{Mv}\\ \dfrac{\mu c_f\ell_f}{I_\Psi}\end{bmatrix}\delta_f, \tag{1}$$

with parameters defined as:

M	vehicle mass
I_Ψ	vehicle inertia about vertical axis at CG
$\ell_f(\ell_r)$	distance of front(rear) axle from CG with $\ell=\ell_f+\ell_r$
d_S	distance between sensor location S and CG along vehicle longitudinal axis
$c_f(c_r)$	nominal front(rear) wheel cornering stiffness
μ	road adhesion as a factor of effective cornering stiffness $c_f^* = \mu c_f$ ($c_r^* = \mu c_r$)

The analysis in later chapters is based on the parameters of one of the cars used in the California PATH project, a 1986 Pontiac 6000 STE sedan, summarized in Table 1.

The transfer function from the steering angle δ_f to yaw rate $\dot{\Psi}$ is given by

$$\dot{\Psi}(s)=\frac{(\mu c_f\ell_f Mv^2)s+\mu^2 c_f c_r\ell v}{\mathcal{D}(s)}\delta_f(s), \tag{2}$$

where $\mathcal{D}(s)$ is the second order denominator

$$\mathcal{D}(s)=I_\Psi Mv^2s^2+v\left(I_\Psi(c_f+c_r)+M\left(c_f\ell_f^2+c_r\ell_r^2\right)\right)s + \mu Mv^2(c_r\ell_r-c_f\ell_f)+\mu^2c_fc_r\ell^2. \tag{3}$$

The *Laplace*-variable is denoted by s. The dynamics of side-slip angle β are

$$\beta(s)=\frac{(\mu c_f I_\Psi v)s+\mu c_f\ell_f(\mu c_r\ell-Mv^2)}{\mathcal{D}(s)}\delta_f(s). \tag{4}$$

Table 1 Car parameters of a 1986 Pontiac 6000 STE sedan.

M	I_Ψ	ℓ_f	ℓ_r	d_S	$c_f=c_r$
1573 kg	2873 kg m^2	1.1 m	1.58 m	1.96 m	80000 N/rad

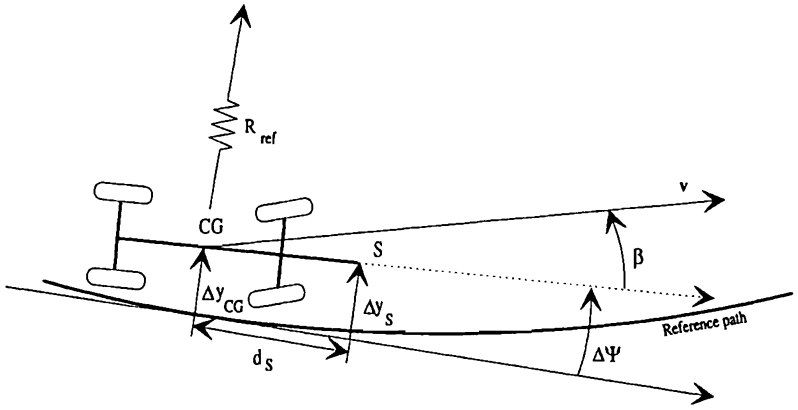

Fig. 2. Vehicle following a reference path.

Yaw rate $\dot{\Psi}$ and side-slip angle β are the two internal states $x = [\beta \ \dot{\Psi}\ ]^T$ of the vehicle dynamics states. Define lateral acceleration $\ddot{y}_S$ at the sensor location S, typically the front bumper, as an output of the system. The transfer function from steering angle δ_f to $\ddot{y}_S$ can be derived as

$$\ddot{y}_S(s) = \frac{\mu c_f v^2(M\ell_f d_S + I_\Psi)s^2 + \mu^2 c_f c_r \ell v(d_S + \ell_r)s + \mu^2 c_f c_r \ell v^2}{\mathscr{D}(s)}\delta_f(s)$$

$$= V_S(s)\delta_f. \tag{5}$$

The front wheel steering angle δ_f is the output of a position controlled actuator with limited bandwidth, denoted by

$$\delta_f = A(s)\delta, \tag{6}$$

where δ is the commanded steering angle.

Fig. 2 shows a vehicle following a circular reference path with a radius R_{ref}. Lateral displacement of the vehicle from the reference path is denoted by Δy_{CG} at CG and by Δy_S at sensor location S. The vehicle longitudinal axis spans the side-slip angle β with the vehicle velocity vector v and the angular displacement error $\Delta\Psi$ with the tangent to the reference path. For convenience, we define the reference curvature as $\rho_{ref} := 1/R_{ref}$.

From above, we extract the plant subsystems: a kinematic system, a (geometric) reference system, and the lateral vehicle dynamics (5) with actuator dynamics (6), all viewed at the sensor location S. The reference system prescribes a lateral acceleration at S of

$$\ddot{y}_{ref} = v^2 \rho_{ref}. \tag{7}$$

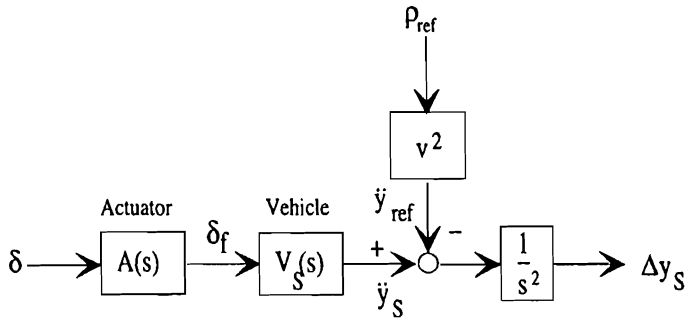

Fig. 3. Block diagram of open-loop steering control system.

The kinematic system reduces to a double integrator for the lateral displacement measurement Δy_S:

$$\Delta y_S = \frac{1}{s^2}(\ddot{y}_S - \ddot{y}_{ref}). \tag{8}$$

The open-loop block diagram for the entire plant is shown in Fig. 3.

2.2. Controller Design Requirements

Control design requirements, as partially discussed in the introduction, include performance, robustness and actuator bandwidth. First, examine the reference input ρ_{ref}. The vehicle speed $v = |v|$ should be chosen to limit the lateral acceleration during steady state curve riding to

$$(a_{ref})_{max} = v^2 \rho_{ref} \leq 0.2g, \tag{9}$$

where $g = 9.81\ m/s^2$ is the gravity constant. The worst-case change in reference curvature is a step input $\Delta\rho_{ref}$ from negative maximum curvature to positive maximum curvature (or visa versa),

$$\Delta\rho_{ref} = 2\frac{(a_{ref})_{max}}{v^2} = 0.4\frac{g}{v^2}. \tag{10}$$

The associated step response of the lateral displacement should be $|\Delta y_S| \leq 0.30$ m in extreme cases, e.g. in the case of a concurrent significant change of the road surface. Under normal driving conditions on US highways, straight line segments are build in-between two opposing curves. In this case, the lateral error should not exceed $|\Delta y_S| \leq 0.15$ m, e.g. for a step input with (9).

For ride comfort, the closed loop system should be well damped to avoid excessive lateral acceleration generated by the controller in addition to the reference acceleration (9). This performance has to be achieved under a wide

range of operating conditions. For the sake of simplicity, we assume all slowly time-varying parameters like car mass, inertia and location of CG are known, e.g. by estimation. Only the road adhesion factor μ is assumed uncertain. Empirical data of various studies suggests an upper bound of $\mu = 1$ for dry road with a good surface, $\mu \approx 0.5$ for wet road and a lower bound of $\mu = 0.1$ for pure ice. Since changes may be abrupt, stability has to be guaranteed without adaptation, at least for subsets of the above range.

A set of "normal" road conditions is defined for $0.5 \leq \mu \leq 1$ for wet or better road. This range is chosen conservatively to include different road surface and tire qualities with varying adhesion factors. Based on the largest reference curvature $(\rho_{ref})_{max}$ on a given stretch of road, the maximal velocity is set by solving (9).

"Adverse" road conditions, e.g. snow and ice, are not considered explicitly here. It is the general assumption that such extreme conditions would either lead to discontinuing operation of automated highways or to significant speed reductions. For illustration purposes, poor road conditions with $\mu < 0.5$ are included in the analysis of the system, but not in the analysis of control design.

Additional design constraints are related to the steering actuator dynamics (6). The necessity of being able to implement an automatic steering system on an average passenger car without major constructional adaptation of currently used steering mechanisms, together with cost and energy consumption considerations, limits the available actuator bandwidth to 5–10 Hz. For control design, actuator dynamics present an additional uncertainty since they vary e.g. with command amplitude. This implies that the actuator cannot be relied upon for control roll-off. The controller to be designed has to provide roll-off itself, taking into account the worst-case actuator dynamics.

3. PROBLEM ANALYSIS

This section is dedicated to the analysis of the plant dynamics. First, we examine the characteristics of the transfer function $V_S(s)$ in (5) in Section 3.1. Second, we separate (5) into the lateral vehicle dynamics at CG and the effect of the look-ahead distance d_S, to study their respective influence in Section 3.2. A comparison between low speed and high speed characteristics of the plant dynamics (5) is presented in Section 3.3. The consequences for control design are later discussed in Section 4.

3.1. Plant Dynamics at Sensor Location S

In the analysis below, speed v is assumed measurable, and hence available for control, but μ is inherently uncertain. A set of Bode plots is shown in Fig. 4 for the lateral dynamics $V_S(s)$ in (5) without the steering actuator (6), using the parameters in Table 1. The left two graphs depict velocity dependency for $10\ m/s \leq v \leq 40\ m/s$ and $\mu = 1$. The right graphs illustrate the influence of $0.1 \leq \mu \leq 1$ at constant speed $v = 40 m/s$. Note that the plot for $\mu = 0.1$ and

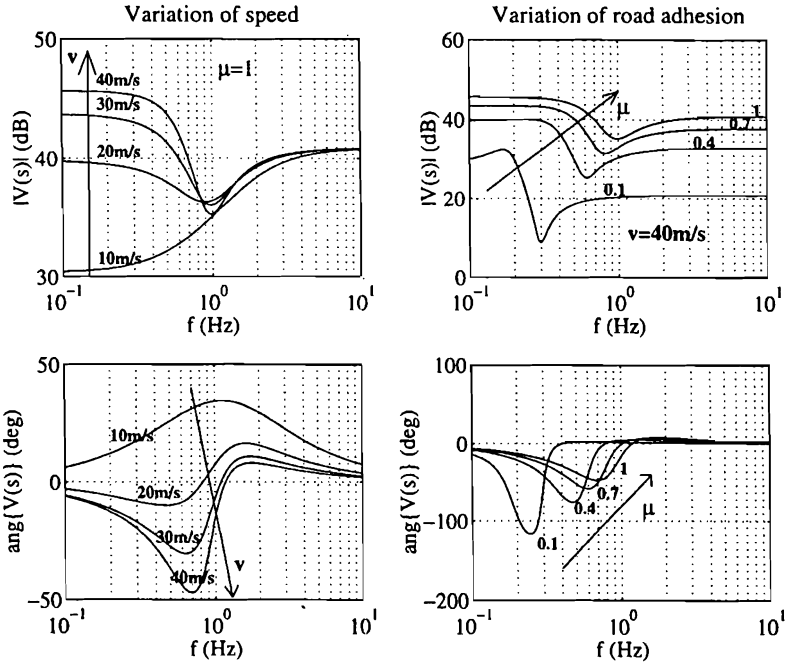

Fig. 4. Bode plots of lateral vehicle dynamics (5) at sensor location S for variation of speed $10 \leq v \leq 40$ m/s on good road $\mu = 1$ (left) and variation of road adhesion $0.1 \leq \mu \leq 1$ at high speed $v = 40$ m/s (right).

$v = 40$ m/s (high speed driving on ice) is shown to illustrate the influence of road conditions on vehicle dynamics rather than to represent a realistic driving situation.

At low frequencies, the steady state gain of the lateral dynamics (5), $V_S(0)$, is

$$V_S(j\omega = 0) = \frac{\mu c_f c_r \ell v^2}{Mv^2(c_r \ell_r - c_f \ell_f) + \mu c_f c_r \ell^2}. \tag{11}$$

The high frequency gain is given by

$$V_S(\infty) = \lim_{\omega \to \infty} V_S(j\omega) = \mu c_f \left(\frac{d_S \ell_f}{I_\Psi} + \frac{1}{M} \right). \tag{12}$$

Observations:

- The natural mode of the vehicle dynamics (5) is negligible for low speed ($v \leq 20$ m/s), but significant for high speed due to notch filter characteristics. The amplitude of the gain variation and hence the phase variation increases with increasing speed and decreasing road adhesion. Furthermore, phase lead is

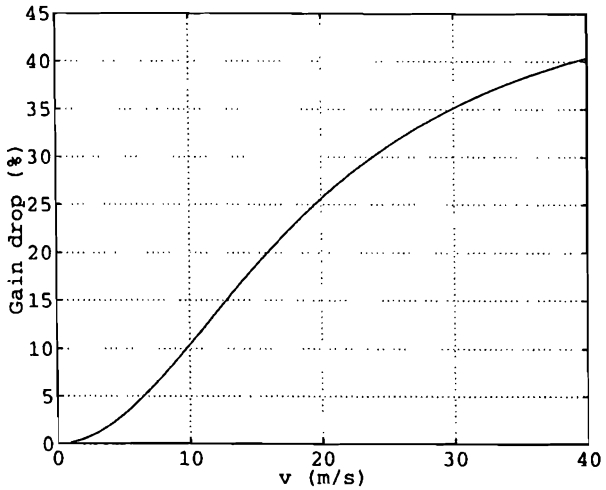

Fig. 5. Percentage drop (%) in steady state gain $|V_S(0)|$ for a change in road adhesion from $\mu = 1$ to $\mu = 0.5$ at different speeds 1 m/s $\leq v \leq$ 40 m/s.

provided for low speed while higher speed features phase lag around the frequency for the natural mode.

- The frequency of the natural mode is "almost" independent of v, but decreases with deteriorating μ.
- The steady state gain $|V_S(0)|$ depends both on v and μ due to understeer characteristics, whereas the high frequency gain $|V_S(\infty)|$ is velocity independent and varies only with μ. The steady state gain dependency on speed follows the basic motion law $\ddot{y} = v^2\rho$ for driving through a circle with $R = 1/\rho$, but is also influenced by understeer characteristics, especially at higher speeds $v > 20$ m/s.
- Dependency of the steady state gain $|V_S(0)|$ on μ is negligible for low speed, but is almost linear at higher speeds. Fig. 5 shows the dependency of the relative drop in gain $|V_S(0)|$ for changing road adhesion from $\mu = 1$ to $\mu = 0.5$. The gain drop can be attributed to understeer characteristics, in particular to the term $(Mv^2(c_r\ell_r - c_f\ell_f))$ in the denominator of (11). Shifting CG to the front, e.g. by seating two passengers in front, increases understeer and hence the gain drop whereas a heavy load in the trunk decreases the effect by shifting CG to the rear.
- For low speed, $|V_S(0)| < |V_S(\infty)|$ and for high speed, $|V_S(0)| > |V_S(\infty)|$, implying that the initial response to a steering angle step will be higher than steady state for low speed, but smaller than steady state for high speed. Hence at low speed, phase lead is provided due to a gain increase, but a phase lag results at higher speed from the gain decrease. While $V_S(0)$ is independent of d_S, $V_S(\infty)$ increases with d_S, reversing the effect of increasing speed.

The locations of the two poles and the two zeros of the lateral acceleration transfer function (5) are shown in Fig. 6 for a speed range of 2 m/s $\leq v \leq$ 40 m/s

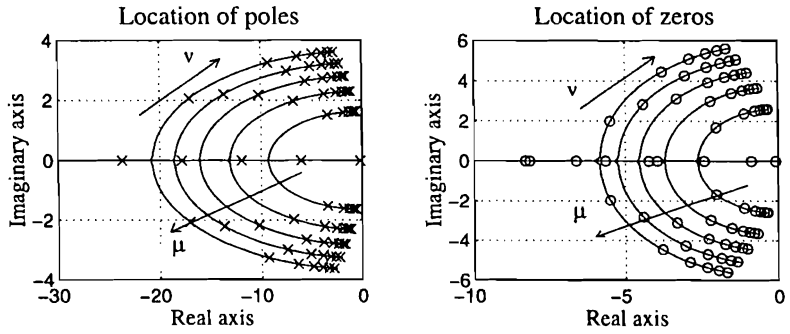

Fig. 6. Poles and zeros of acceleration transfer function (5) for variation in v and μ.

and five different road adhesion factors $\mu = 0.2, 0.4, \ldots, 1$. After splitting on the real axis, both the poles and the zeros move with increasing speed on circular arcs towards the imaginary axis, without ever crossing it. Increasing μ magnifies the circles of the poles and zeros, which corresponds to higher natural frequencies as seen in Fig. 4.

Fig. 7 shows the dependency of numerator (zeros) and denominator (poles) damping, respectively, on v and μ. Both damping coefficients decrease with

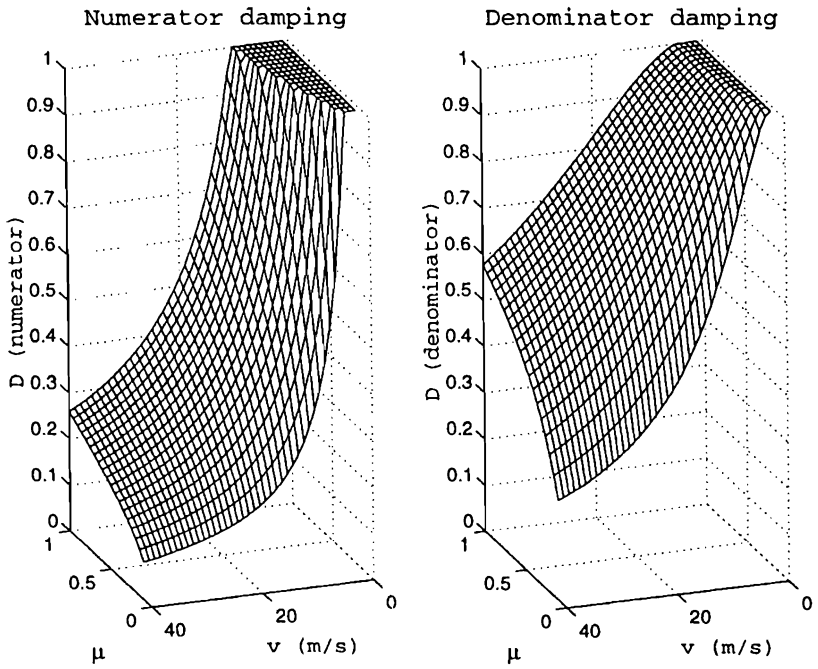

Fig. 7. Damping coefficients of the zero-pair and pole-pair of the lateral acceleration transfer function (5) for varying speed $1 \leq v \leq 40$ m/s and the full range of road adhesion $0.1 \leq \mu \leq 1$.

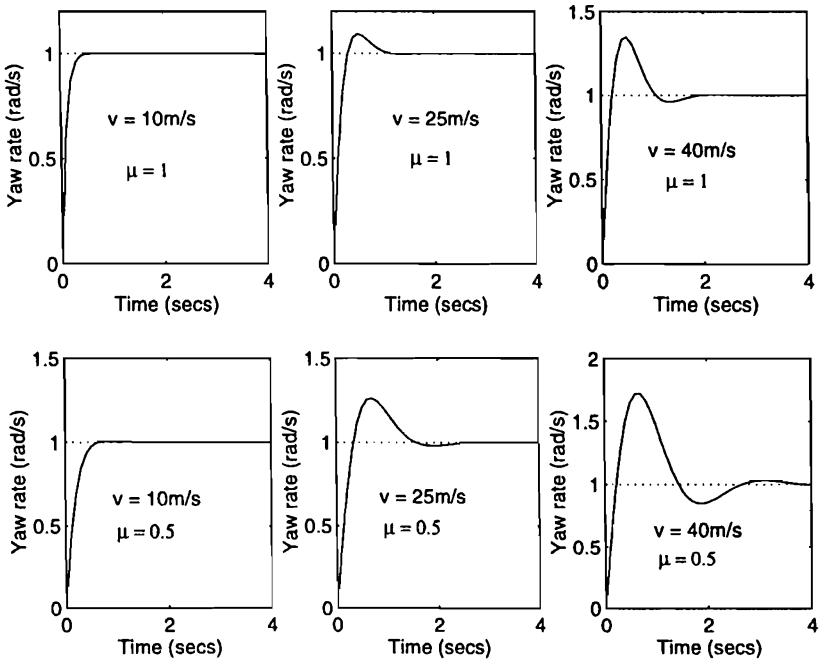

Fig. 8. Step responses in vehicle yaw rate for different values of v and μ, normalized to steady state $\dot{\Psi}(t \to \infty) = 1$ rad/s.

increasing speed and decreasing road adhesion, the zeros to even lower values than the poles. Decreasing damping for increased velocity and decreased road adhesion results in overshoot and oscillatory behavior in the step responses of yaw rate $\dot{\Psi}$ and lateral acceleration $\ddot{y}_S$. Consider the normalized yaw rate responses for a step in δ_f in Fig. 8 for six different speeds and road conditions. Overshoot increases with velocity to about 40% on a dry road ($\mu = 1$) and even to 70% for $\mu = 0.5$ on wet road at $v = 40$ m/s. Low damping of the poles leads to significantly oscillatory behavior for higher speeds, again deteriorating with decreasing road adhesion μ.

For the last part of the analysis of vehicle dynamics, re-arrange (2)–(5) to the form $\ddot{y}_S = Cx + Du$ with the internal states $x = [\beta \quad \dot{\Psi}]$ and input $u = \delta_f$:

$$\ddot{y}_S = \mu\left(\left(\frac{d_S(c_r\ell_r - c_f\ell_f)}{I_\Psi} - \frac{c_r + c_f}{M}\right)\beta + \frac{1}{v}\left(-\frac{d_S(c_f\ell_f^2 + c_r\ell_r^2)}{I_\Psi} + \frac{c_r\ell_r - c_f\ell_f}{M}\right)\dot{\Psi} + \left(\frac{d_S c_f \ell_f}{I_\Psi} + \frac{c_f}{M}\right)\delta_f\right). \tag{13}$$

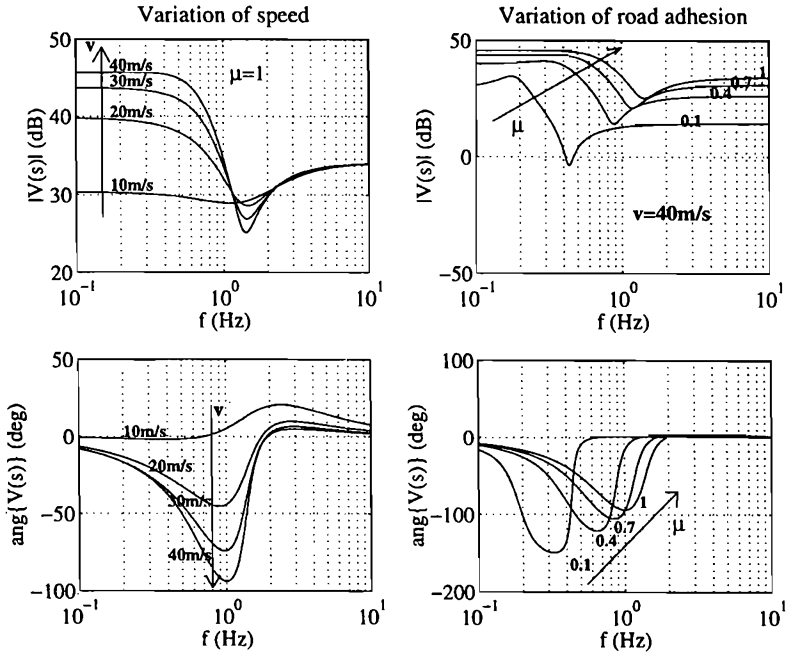

Fig. 9. Bode plots of lateral vehicle dynamics at CG for variation of speed $10 \leq v \leq 40$ m/s on good road $\mu = 1$ (left) and variation of road adhesion $0.1 \leq \mu \leq 1$ at high speed $v = 40$ m/s (right).

The contribution of yaw motion to lateral acceleration diminishes by the inverse of v (see second line of (13)), in favor of side-slip β, in compliance with basic motion laws. This means that cars are "drifting sideward" rather than yawing during cornering at higher velocities. Due to the direct relationship between effective cornering stiffnesses $c_f^* = \mu c_f$ and $c_r^* = \mu c_r$, and the side-slip proportional lateral force, dominance of side-slip over yaw motion at high speed leads to stronger dependency of the lateral acceleration gain on road adhesion μ as already shown in Fig. 5. Note that lateral acceleration $\ddot{y}_S$ directly describes the lateral motion of sensor location S and hence is the direct control variable for the automatic steering system in Fig. 3.

3.2. Influence of Look-Ahead Distance d_S

The lateral acceleration at sensor location S can be written as

$$\ddot{y}_S(s) = \ddot{y}_{CG}(s) + d_S\ddot{\psi}(s), \tag{14}$$

where $\ddot{y}_{CG}(s) = V_{CG}(s)\delta_f(s)$ is the lateral vehicle acceleration at CG obtained by setting $d_S = 0$ in (5) and $\ddot{\psi}(s)$ is the yaw acceleration obtained by differentiating (2). Bode plots for the two components are shown in Figs. 9 and 10 for similar operating conditions as in Fig. 4.

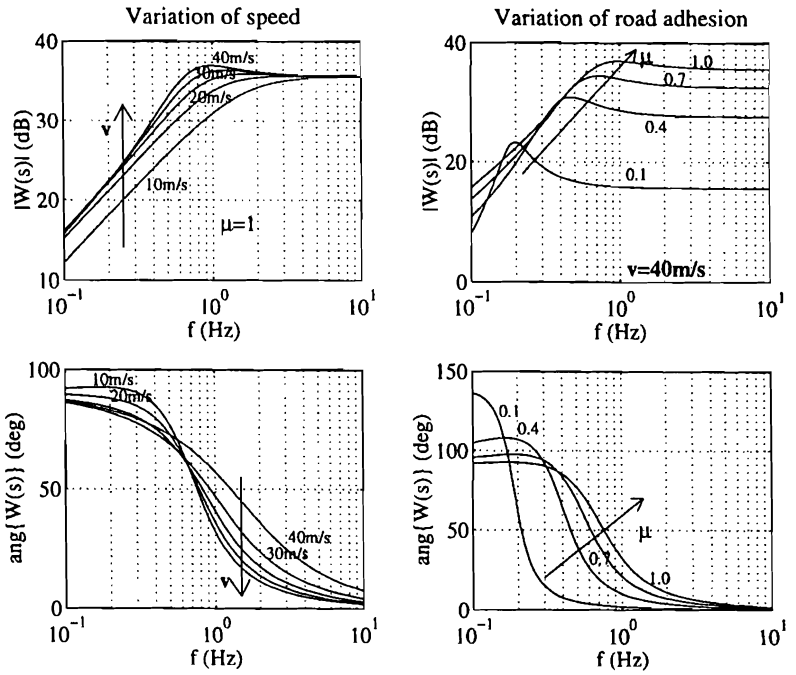

Fig. 10. Bode plots of yaw acceleration $W(s) = (d_S \ddot{\Psi}(s)/\delta_f)$ with $d_S = 1.96$ m for variation of speed $10 \leq v \leq 40$ m/s on good road $\mu = 1$ (left) and variation of road adhesion $0.1 \leq \mu \leq 1$ at high speed $v = 40$ m/s (right).

The lateral vehicle dynamics $V_{CG}(s)$ at CG feature a distinct gain change with a second order notch characteristic in the range 0.5–3 Hz. As already observed in Section 3.1, a gain increase occurs for low speed due to $|V_{CG}(0)| < |V_{CG}(\infty)|$, whereas high speed experiences a significant gain decrease according to $|V_{CG}(0)| > |V_{CG}(\infty)|$. Phase lead is associated with gain increase, but phase lag results from gain decrease.

Physically, lateral acceleration at CG is entirely generated by the steering angle δ_f and side-slip angle β via respective forces at the tires. At low speed, side-slip counteracts steering and hence yields a steady state gain lower than the high frequency gain. On the other hand, side-slip adds to the steering angle at higher speed ($v > 14$ m/s), resulting in an increasing gain and hence a steady state gain greater than the direct throughput of δ_f determined by the high frequency gain. Poor damping of the zero-pair of $V_{CG}(s)$ creates a shaper phase drop than associated with the sole gain drop and additionally results in gain "undershoot" with $|V_{CG}(j\omega)| < |V_{CG}(\infty)|$ between 1 and 2 Hz.

Decreasing road adhesion magnifies the variation of steady state gain and adds variation of the high frequency gain. Furthermore, the effect of the natural mode of the vehicle dynamics increases, causing an even shaper phase drop than for $\mu = 1$. Concurrently, the frequency of this mode decreases with decreasing μ

together with the range of the gain variation. This is to be expected since μ directly influences the lateral forces generated by steering angle δ_f and side-slip angle β to produce lateral acceleration at CG. Hence, the lateral gain decreases for lower μ over all frequencies and dynamic responses become slower.

The yaw acceleration dynamics, $(\ddot{\Psi}(s)/\delta_f)$, shown in Fig. 10 at sensor S as $W(s) = (d_S\ddot{\Psi}(s)/\delta_f)$, have a DT_1 characteristics with the vehicle mode discussed above around 1 Hz on good road ($\mu = 1$) and decreasing frequency for decreasing μ. For low speeds $v \leq 20$ m/s, the gain of yaw acceleration $(\ddot{\Psi}(s)/\delta_f)$ varies almost linearly with speed v, compared to a quadratic speed dependency of the lateral acceleration gain. For higher velocities, variation of v has little influence on the gain of yaw acceleration while the lateral acceleration gain depends almost linearly on v. However, yaw dynamics experience comparable gain variation due to changes in μ as $V_{CG}(s)$. The D-characteristic for low frequencies results in phase lead up the corner frequency ω_Ψ of the yaw mode, sustaining slightly longer for high speed than for low speed. Decreasing μ, however, decreases the phase lead range by decreasing ω_Ψ.

Adding $\ddot{y}_{CG}(s)$ and $(dS\ddot{\Psi}(s))$ to form $\ddot{y}_S(s)$ in (14) is non-trivial for using Bode plots. We restrain from switching to more appropriate Nyquist plots for the sake of a uniform presentation and confine the discussion to qualitative argumentation. In the low frequency range, $\ddot{y}_{CG}(s)$ dominates over $(d_S\ddot{\Psi}(s))$ in (14) due to the D-characteristic of $\ddot{\Psi}(s)$. At some frequency ω_0, $|\ddot{y}_{CG}(s)|$ and $|d_S\ddot{\Psi}(s)|$ reach comparable magnitudes. Henceforth, phase lag in $\ddot{y}_{CG}(s)$ is compensated partially by phase lead of $\ddot{\Psi}(s)$ for $\omega > \omega_0$, up to the corner frequency ω_Ψ of $\ddot{\Psi}(s)$. The high frequency gain for $\omega \geq \omega_\Psi$ of $V_S(s)$ in (14) is the direct sum of $|\ddot{y}_{CG}(j\omega)| + |d_S\ddot{\Psi}(j\omega)|$, since both phases are approximately equal to zero.

At this point, the significant influence of the look-ahead distance d_S is revealed: By directly determining ω_0 via (14), d_S affects both the range of phase lead provided by $(d_S\ddot{\Psi}(s))$ and the extent to which $|\ddot{y}_S(j\omega)|$ increases over $|\ddot{y}_{CG}(j\omega)|$. Since the gain dependency of $V_{CG}(s)$ is quadratic in v, but linear in v for $\ddot{\Psi}(s)/\delta_f$, a proportional increase of d_S with v would be necessary to compensate the dynamics (14). Look-ahead distance d_S, by describing the output location, directly influences damping of the zeros of transfer function (5), but obviously does not alter the system poles. Damping D_z of the zeros is depicted in Fig. 11 as a function of d_S for $v = 10$, 20, 30, and 40 m/s and $\mu = 0.5$.

Note that damping D_z of the zero-pair directly determines the gain "undershoot" between 1 and 2 Hz, and the distribution of phase lag/lead in this frequency range. Conversely, prescribing a fixed maximum phase lag of the combined lateral acceleration transfer function (5) yields look-ahead requirements for different speeds. A selection of maximum phase lag lines are displayed in Fig. 12 for 10 m/s $\leq$ $v \leq 40$ m/s and worst-case $\mu = 0.5$. A look-ahead distance increase proportional to velocity reduces the phase lag in $V_S(s)$.

It should be noted that for a number of applications of automatic steering control, distance d_S is inherently limited even for look-ahead systems like vision. For example, detection of lane markers with vision sensors is degraded by adverse

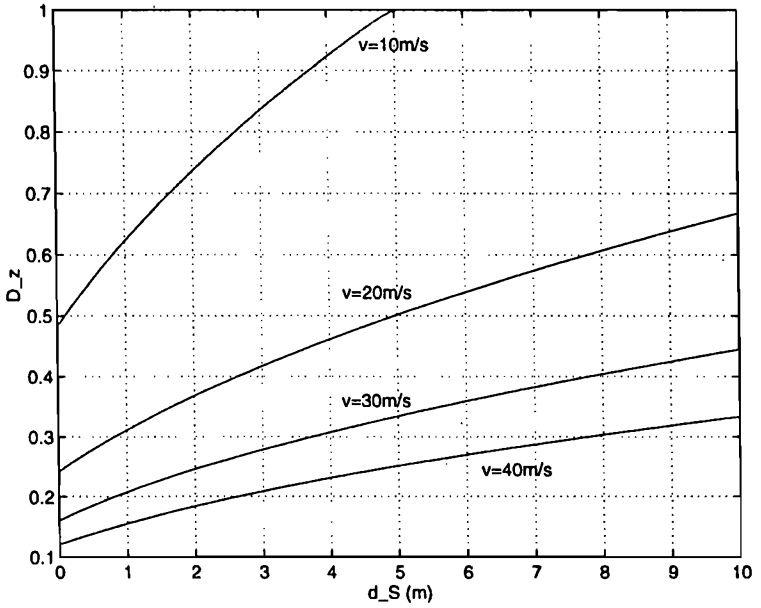

Fig. 11. Damping of the zero-pair of the lateral acceleration transfer function $V_S(s)$ in (5) as a function of look-ahead distance d_S for different velocities on a poor road surface $\mu = 0.5$.

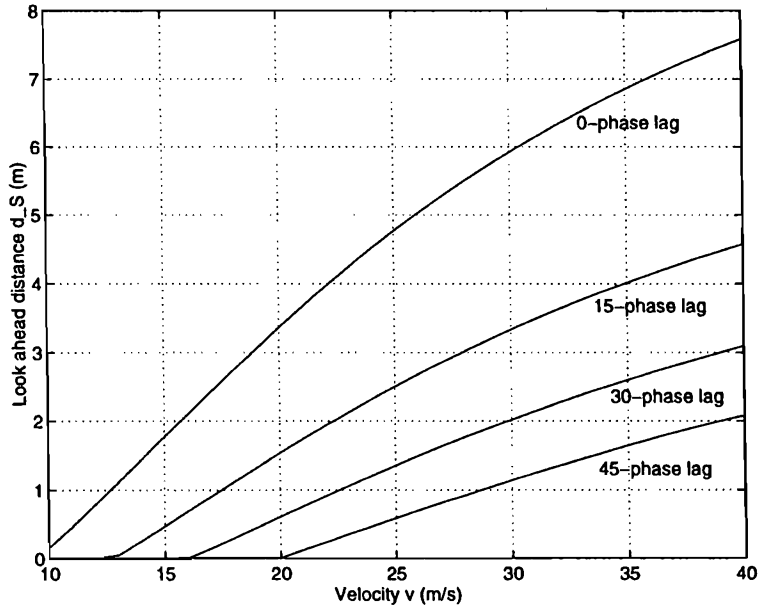

Fig. 12. Look-ahead distance d_S requirements for prescribed maximum phase lag a on poor road surface $\mu = 0.5$ for speed variation 10 m/s $\leq$ v $\leq$ 40 m/s.

weather conditions and abrupt light changes (underpasses etc.). Furthermore, for automated highway systems (AHS) using platooning with close inter-car spacing [3], preceding vehicles will severely obstruct the field of view, limiting the available look-ahead distance at best to twice, maximum three times the vehicle spacing for detecting side markings of the road. Consequently, control design for small d_S is vital for practical automatic steering, independently of the reference system being used.

3.3. Comparison: Low and High Speed

In this subsection, we contrast automatic steering control for a look-down reference system at low speed and at high speed. "Low speed" characterizes driving in residential areas, below 30 mph (13.4 m/s). A velocity of $v_{lo} = 10$ m/s is picked as an example representing low speed. "High speed", on the other hand, describes highway driving above 55 mph (24.6 m/s), here represented by the example of $v_{hi} = 40$ m/s.

3.3.1. Vehicle dynamics at CG

At low speed, the vehicle dynamics are well damped and can be treated as a "static" P-transfer function, with a steady state gain depending only slightly on road adhesion μ. For increasing velocity, damping of both zeros and poles decreases and leads to overshoot and oscillations in step responses, see Figs. 7 and 8. The associated phase lag in the range of the notch frequency of the vehicle (at approximately 0.5–0.9 Hz for the parameters of the Pontiac 6000 STE in Table 1) has to be accounted for in the control design. Furthermore, the steady state gain depends almost linearly on μ at high speed.

3.3.2. Influence of look-ahead distance d_S

The lateral acceleration at sensor location S is a linear combination of lateral acceleration at CG and yaw acceleration ($\ddot{\Psi}(s)/\delta_f$) multiplied by look-ahead distance d_S. At low speed, small d_S in the order of half a vehicle length as found in look-down systems suffices to provide phase lead due to comparable magnitudes of lateral acceleration at CG and yaw acceleration. On the other hand, lateral acceleration at CG dominates over yaw acceleration for fixed, small d_S at high speed due to quadratic dependency on v of gain $|V_{CG}(s)|$ compared to linear speed-dependency of yaw acceleration.

3.3.3. Control design requirements

The lateral control problem has been solved and experimentally verified for low speed with several different control approaches. Independent of the control design technique used, all output-feedback controllers known to the authors have a general frequency characteristic in common. A zone of moderate proportional gain in the mid-frequency range is generally flanked by an integral zone in the low frequency range for zero steady state errors and by a differentiating frequency zone around cross-over to provide sufficient phase margin for stabilization and comfortable damping. Roll-offs with T_n-low pass characteristics usually meet

actuator bandwidth limitations. Such $PIDT_n$-type control is only feasible for low speed due to the absence of phase-lag introduced by the vehicle dynamics as illustrated in Fig. 9. In fact, for large enough look-ahead distance d_S, the car dynamics $V_S(s)$ themselves provide phase lead, which can be utilized for stabilization, reducing the controller requirement to PIT_n control.

For highway speed, two additional issues have to be addressed by control design: compensation of phase lag introduced by poorly damped car dynamics with an increasing dominance of the zero-pair and the diminishing phase lead provided by look-ahead d_S. Decreasing car damping prohibits continuing integral action in this frequency range and, on the contrary, requires phase lead from the controller for sufficient damping. The necessity to stabilize the double-integrator by a strong differential term calls for at least a $PIDD^2$ structure with an additional compensator for the car dynamics. However, in order to fulfill the robustness requirements with respect to μ, "over compensation" is required. This leads to strong, continued requirement of phase lead, which inevitably results in high gain above the 1 Hz range, colliding with the phase lag of the actuator dynamics and noise considerations. Furthermore, since exact compensation of the car dynamics is impossible, their influence of being in the close vicinity of controller roll-off will prevail in closed-loop, requiring delicate fine-tuning to guarantee sufficient damping for the full range of $0.5 \leq \mu \leq 1$.

	Low speed	**High speed**
Car dynamics	negligible; dominated by yaw motion	low damping ⇒ overshoot, oscillations; dominated by side-slip
Car gain $V_S(0)$	little dependency on μ	(almost) linear dependency on μ
Small look-ahead d_S	provides phase lead for control	phase lead smaller than vehicle lag
Actuator dynamics	away from control frequency range	close to control frequency range
Control tasks	· rejection of disturbance input ρ_{ref} · ride comfort	· rejection of disturbance input ρ_{ref} · compensation of car dynamics · robustness for car gain variation · ride comfort · **stability** (actuator dynamics etc.)
Controller structure	PID	$PIDD^2$ + compensation for car dynamics, **but** constrained by actuator dynamics

4. OUTPUT FEEDBACK CONTROL

The previous section already touched upon some issues of output feedback control design. We will subsequently detail the requirements for control design by stepwise consideration of control tasks.

4.1. Preliminary Remarks

The discussion in this section is founded entirely on linear control argumentation, mainly in the frequency domain. We regard a linear control design as the basis for

a possibly more involved design using nonlinear techniques. Any nonlinear controller, however, can be linearized around the operating point, e.g. $\Delta y_S = 0$ for any constant μ and v. Such a linearized version of a nonlinear controller must, however, satisfy all stability requirements and should at least partially fulfill performance requirements. Note that this holds both for analytical nonlinear techniques like sliding mode and for more heuristic methods like fuzzy and neural-network control. Any controller, linear or nonlinear, will rely on the available information content of the feedback signal. Hence, linear methodology is the appropriate tool to study possible design directions, providing the basis for future more involved designs using some of the above mentioned methods.

Adaptation and estimation techniques operate on time scales below the system time constants. As mentioned in Section 2, all parameters are assumed constant except road adhesion μ, which may change abruptly. Hence, no "slowly time-varying" assumptions hold and true robustness is required to simultaneously stabilize the full range of $0.5 \leq \mu \leq 1$. For improving performance after the basic control design, estimation/adaptation will be useful to identify and cope with variations in the remaining system parameters. Such schemes, however, would not significantly improve stability. On the contrary, estimation/adaptation schemes lead to a more difficult stability analysis. Similar argumentation holds for predictive control, which tries to predict future plant behavior based on the current state of the plant, a dynamic plant model, and knowledge of future reference inputs. All available information of earlier outputs is represented in the lower frequency range of the output measurement and hence would be used e.g. in an integral term. Predicting the future, however, relies on knowledge of the vehicle dynamics which are highly uncertain due to μ.

4.2. Performance and Stability Requirements

First, the design requirements for the closed loop system

$$\Delta y_S(s) = H(s)\rho_{ref} \tag{15}$$

have to be interpreted. The performance requirement for "normal operation" of less than $(\Delta\ y_S)_{max} = 0.15$ m error for a step input in road curvature of $(\Delta\rho_{ref})_{max} = (a_{ref})_{max}/v^2$ in (9) translates into a gain requirement for the closed loop transfer function H(s),

$$|H(s)| \leq \frac{(\Delta y_S)_{max}}{|(\Delta\rho_{ref})_{max}|}, \forall s. \tag{16}$$

This estimation is based on the inequality

$$|\Delta y_S(t)| = |\mathcal{L}^{-1}\left\{H(s)\frac{1}{s}(\Delta\rho_{ref})_{max}\right\}| \leq |H(s)| \cdot |(\Delta\rho_{ref})_{max}|, \tag{17}$$

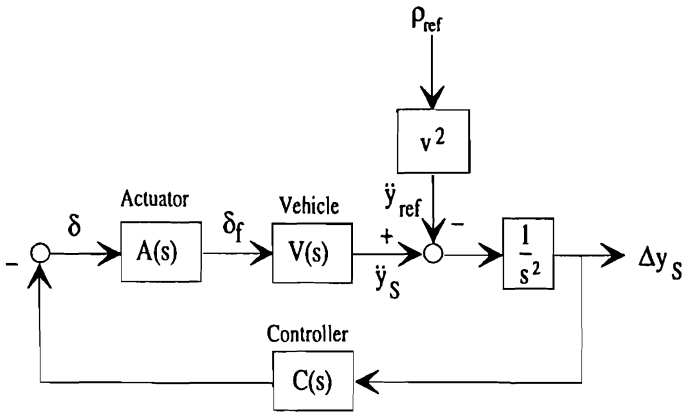

Fig. 13. Block diagram of an output feedback steering control system.

where $\mathcal{L}^{-1}\{\cdot\}$ denotes the inverse Laplace-transform. From the sketch of the closed loop system in Fig. 13 using output feedback for lateral control, we read

$$H(s) = \frac{v^2}{s^2 + C(s)A(s)V_S(s)}, \tag{18}$$

with $V_S(s)$ denoting the lateral car dynamics (5), A(s) describing the actuator dynamics (16), and C(s) being the controller to be designed.

As a first step, let $V_S(s) = V_S(0)$ (given by (11)) and $A(s) = 1$ in (6), i.e. a car without dynamics and with an ideal steering actuator, considering only variation of the steady state gain. For comparing $v_{lo} = 10$ m/s and $v_{hi} = 40$ m/s, we choose $\rho_{ref} = (a_{ref})_{max}/v_{hi}^2$, yielding a reference radius of $R_{ref} 1/\rho_{ref} = 815.5$ m. The performance bound (16) for closed loop (18) is solved for output feedback controller $C(s) = |C(j\omega)|\exp(j\alpha(\omega))$. Contour-plots for phase lead $\alpha(\omega) = 0°$, 60°, 120°, and 180° are shown in Fig. 14 for $v_{lo} = 10$ m/s (left graphs) and $v_{hi} = 40$ m/s (right graphs), with respective $\mu = 1$ (top graphs) and $\mu = 0.5$ (bottom graphs).

The dashed "stability line" represents the inverse plant dynamics, in the case of Fig. 14 a double differentiator with gain $1/V_S(0)$. At low frequencies, the controller $C(j\omega)$ is requiring a gain $|C(j\omega)|$ *above* the 0°-phase performance line. When crossing the stability line, an appropriate phase margin is necessary, e.g. $\approx 60°$ for critical damping. After the cross-over, the performance requirements can be disregarded.

In order to achieve the basic performance requirements, a PD-controller of the type

$$C(s) = K\frac{T_d}{T_n} \cdot \frac{s + T_n}{s + T_d}, \quad T_n < T_d \tag{19}$$

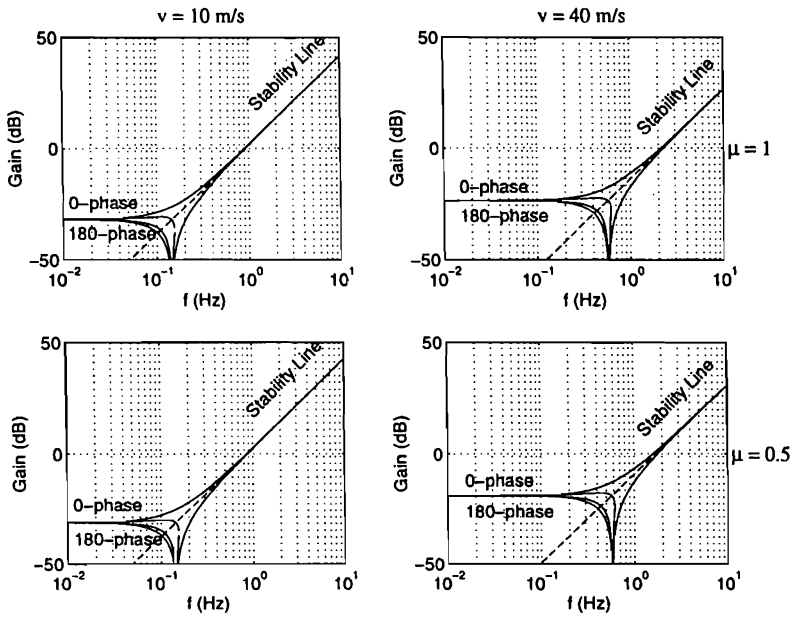

Fig. 14. Performance requirements for C(s) without car and actuator dynamics.

suffices for appropriate $K = C(0) \geq \frac{(\rho_{ref})_{max}}{(\Delta y_S)_{max}} \frac{v^2}{V_s(0)}$. Both the gain requirement for C(0) and the possible cross-over frequency increase with increasing speed v. Although not demonstrated in Fig. 14, it can be shown that this effect is reversed for driving through curves with smaller radii at lower velocity, keeping $(a_{ref})_{max}$ constant.

The need to provide good damping by having approximately 60°-phase lead around the cross-over frequency (≈ 1 Hz at $v = 40$ m/s) requires $T_n \approx 10T_d$, resulting in almost 20 dB gain increase for higher frequencies, i.e. $C(\infty) \approx 10C(0)$. Higher order filters instead of (19) with sharper phase increases may result in smaller gain increases (about 10 dB for a fourth-order filter). However, since the variation of the vehicle gain V(0) due to μ creates a frequency range of possible cross-overs, phase lead has to be provided for this whole range rather than for a single cross-over point.

"High" $C(\infty)$ is undesirable due to noise characteristics, but does not conflict with actuator dynamics in the above case due to a "low" cross-over frequency which leaves sufficient room for roll-off. An integral term K_I/s can be added to (19) to obtain zero steady state error, with K_I chosen such that the cross-over 60°-phase margin is not jeopardized.

As a second step, consider the full vehicle dynamics V(s) of (5), but still without actuator dynamics (6). The controller gain requirements are shown in Fig. 15, in a similar manner as in Fig. 14. For low speed ($v = 10$ m/s), the

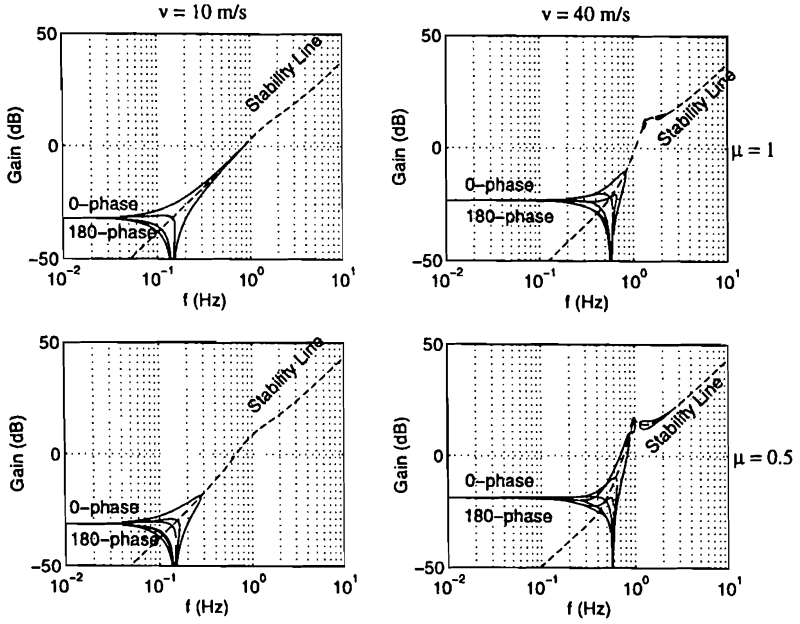

Fig. 15. Performance requirements for C(s) with car dynamics, but without actuator.

requirements are similar to Fig. 14 as expected from the studies in Section 3.1. For high speed, however, the vehicle dynamics require attention. First, the slope of the stability line increases in the 1 Hz region, resulting in severe phase lag in addition to the 180°-lag of the double integrator, complicating cross-over. Second, the phase lag associated with the notch characteristics of transfer function (5) (also see Fig. 4) would cause poor damping of the closed loop when using controller (19), especially at decreased road adhesion $\mu = 0.5$. Hence, an additional phase lead has to be introduced, e.g. by an additional second order lead-compensator

$$C^*(s) = C(s)\frac{\lambda_d^2 s^2 + 2D_n\lambda_n s + \lambda_n^2}{\lambda_n^2 s^2 + 2D_d\lambda_d s + \lambda_d^2}, \quad \lambda_n < \lambda_d \tag{20}$$

Since the additional phase requirement is of the same order as for stabilization of the double integrator in Fig. 14, a significant additional gain increase by λ_d^2/λ_n^2 to $C(\infty)$ is the consequence. Third, the robustness requirement to compensate the vehicle dynamics by providing phase lead for all possible $0.5 \leq \mu \leq 1$ leads to "over compensation". Hence, the gain increase is not fully compensated by simultaneous gain drop in the vehicle dynamics (5) as described by (11) and (12). Furthermore, variation of car gain at higher frequencies (see $V(\infty)$ in (12)) is linear in μ, effectively resulting in an uncertainty factor of 2. The uncertain lateral acceleration gain leads to a band of possible cross-over frequencies for which sufficient phase lead has to be provided.

In addition to the obvious noise rejection concerns of using "high" gain at high frequencies, actuator dynamics play an increasingly important role. "Higher" gain at high frequencies increases the cross-over frequency, in fact into the range of actuator dynamics of type (6) with bandwidth limitations of 5–10 Hz. In addition, high frequency measurement noise is amplified significantly.

We conclude from the above that automatic steering control for highway speed based on output feedback is impractical under the given performance requirements and design constraints.

5. EVALUATION OF DESIGN ALTERNATIVES

The inadequacy of pure output feedback under the given practical constraints illustrates the need for additional measures. Several options are available to aid in feedback control or to modify the system structure. The following subsections will discuss the respective benefits and associated practical issues.

5.1. Preview of Road Curvature

So far, road reference curvature ρ_{ref} has been regarded as an unknown disturbance input to the plant in Fig. 3. Some lateral reference systems for highway automation allow transmission of a road curvature preview to the vehicle. For example, binary polarity coding can be used in the magnetic marker system developed at California PATH [7]. On a geometric level, knowledge of the input $\rho_{ref} = 1/R_{ref}$ is exact. In combination with vehicle speed v, a reference yaw rate $\dot{\Psi}_{ref}$ and a reference lateral acceleration $\ddot{y}_{ref}$ (at CG) can be computed as in (7).

Due to the uncertain gain of the car dynamics (5), especially noticeable for high speed caused by variation of μ, direct feed-forward of a reference steering angle is inaccurate. The road curvature represents "only" the future reference signal, and has to be coupled with predictions of future car behavior to generate a preview-based feed-forward. Prediction, therefore, is not exact due to inherent model uncertainty. Furthermore, feed-forward using preview of road curvature does not simplify the stabilization problem itself. Nevertheless, for $0.5 \leq \mu \leq 1$, a fixed parameter feed-forward with μ_{ave} substantially decreases the effect of the road curvature disturbance ρ_{ref} and improves performance.

5.2. Feedback of Vehicle Absolute Motion

Affordable sensors to measure vehicle absolute motion, e.g. yaw rate and lateral acceleration, are now available thanks to advances in micro-mechanics. Both variables describe the absolute motion of the vehicle, in contrast to the relative measurement of lateral displacement. Feedback of absolute motion variables may modify the pole locations of the vehicle transfer function (3).

Actuator bandwidth limitations, noise considerations and coupling of other vehicle motions like body roll with yaw and lateral acceleration constrain feedback design. More important, however, the zeros of $V_S(s)$ in (5) with poor damping for high speed v have been identified in Sections 3 and 4 to be the true obstacles for

lateral control design. In short, the zeros attract a pair of system poles in any closed loop for Δy_S, leading to low damping of closed loop poles. Although "closeness" of poles and zeros in closed loop would lead to an (almost) cancellation of their respective effects when viewed at sensor location S, low damping of the poles is highly undesirable. The poles are present in all vehicle transfer functions, with their effect not being compensated by the zeros of lateral acceleration at S. For example, the vehicle yaw rate transfer function (2) features only one real zero, leading to yaw oscillations for poorly damped closed-loop poles.

Despite their limited utility for feedback, measurement of vehicle states is beneficial for secondary control tasks like monitoring of system operation for failure detection and estimation/adaptation for performance improvement. Furthermore, when combined with preview of road geometry, absolute measurements can (theoretically) be transformed into relative variables, at least on a velocity-scale (yaw rate) or acceleration scale. The practical potential of such relative variables obtained by differencing two absolute variables for control on position scale (lateral displacement) remains to be verified.

5.3. Modification of System Zeros

The system zeros of $V_S(s)$ in (5) are determined by sensor location S. In particular, the distance d_S between sensor S and vehicle CG has been shown to be crucial in Section 3.2. An increase of d_S proportional to speed v seems to be required – an observation known from human driving. Most importantly, modification of d_S changes the location of zeros in $V_S(s)$, unlike feedback of motion variables as discussed above. One obvious remedy is to focus on look-ahead reference systems like vision or radar. However, in addition to reliability issues for poor weather conditions of vision systems, long look-ahead is not feasible for highway automation with platooning due to occlusion by preceding vehicles.

The benefits of look-down systems can be preserved while accommodating look-ahead requirements. Complementing a lateral displacement sensor S at the front bumper by a second displacement sensor T, preferably placed at the tail of the vehicle, allows to extrapolate the displacement measurement forward to a virtually increased look-ahead distance d_v beyond the vehicle boundaries. Fig. 16 shows an example of a forward extrapolation of distance d_V to a virtual position y_V. The front lateral displacement, d_S in front of the vehicle's CG, is denoted by

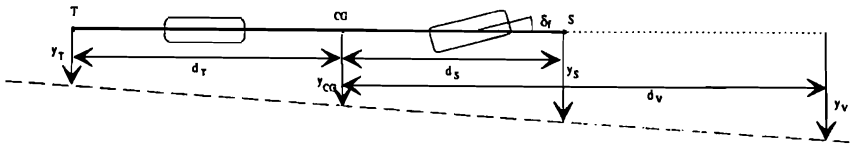

Fig. 16. Forward extrapolation for virtual look-ahead distance d_v of a look-down reference system by using an additional lateral displacement sensor T at the tail of the vehicle.

y_S. The tail lateral displacement, d_T behind CG, is denoted by y_T. Virtual displacement y_V can be calculated via

$$y_V = \frac{(d_V + d_T)y_S - (d_V - d_S)y_T}{d_S + d_T}, \tag{21}$$

assuming $R_{ref} \gg (d_S + d_T)$. Although noise considerations limit virtual look-ahead distance to very few car lengths, this approach is able to satisfy the requirements for look-ahead distance depicted in Figs. 11 and 12 for the full speed range of US highways. Note that a tail displacement sensor T measures a relative variable on position scale, compared to measurement of absolute variables by above discussed inertial sensors for yaw rate (velocity scale) or lateral acceleration (acceleration scale). Furthermore, the measurements can be supported by a Kalman filter structure using measurement of absolute vehicle motion and road curvature preview as discussed above.

6. CONCLUSIONS

Automatic steering control for passenger cars, as an integral subsystem of automated highway systems, has been studied by using various methods of control design. Two different reference system approaches were employed in previous research: "look-ahead" and "look-down". Look-ahead systems determine the vehicle lateral displacement from the desired path at some distance in front of the vehicle. This coincides with human behavior and has been replicated using machine vision or radar by a number of research groups. Look-down systems, on the other hand, measure the lateral displacement at a location within the vehicle boundaries, typically at the front bumper.

In all experiments known to the authors, look-down systems were restricted to low speed (less than 40 mph) under practical conditions. The general assumption was to be able to easily extend the results to highway speed (above 50 mph) by appropriate tuning of control parameters. In this paper, we have shown that fundamental barriers exist for driving at highway speed, which requires complete re-thinking of control design for look-down systems. The barriers are attributed to changes of vehicle dynamics as well as to practical constraints and performance requirements.

The vehicle transfer function from steering angle to lateral displacement at the front bumper consists of a complex zero-pair, a complex pole-pair and a pole-pair at the origin (double integrator). Both the complex zeros and the complex poles experience decreased damping for increasing velocity and deteriorating road surface quality, the zeros even more dramatically than the poles. Due to the combination of the zeros and poles, the vehicle lateral displacement transfer function has a notch-filter characteristic with significant phase lag at higher speeds.

System performance requirements include robustness with respect to sudden changes of road adhesion (e.g. from wet to dry road and back when passing under a bridge), maximum lateral displacement error, and closed loop damping requirements for safety and comfort, all within constraints imposed by practical actuator bandwidth limitations. Under these conditions, pure output-feedback control was shown to be limited to low speed, independent of the control design methodology to be used. Obviously, feedback control may only alter the system poles. When closing the control loop, the poorly damped complex zero-pair attracts a complex pole-pair. Although the effect of consequent poor pole damping does not surface directly in the lateral displacement transfer function due to pole/zero cancellation, it appears in oscillatory yaw behavior. The yaw rate transfer function has the same complex pole-pair as lateral displacement, but only one real zero, and hence no cancellation of poorly damped poles.

We conclude the paper by emphasizing the necessity to alter the system zeros by modifying the system output. This can be done most effectively by increasing the look-ahead distance between the vehicle center of gravity (CG) and the location of the lateral displacement measurement. For look-down reference systems, in addition to the sensor at the front bumper, a lateral displacement sensor should also be installed at the tail of the vehicle to extrapolate a virtual lateral displacement at some distance in front of the vehicle, outside its true physical boundaries. Such a second displacement sensor at the tail enables to preserve the benefits of look-down reference systems while providing the look-ahead ability necessary for control design. Future work will concentrate on the influence of look-ahead distance and on specifics of control design for an experimental vehicle.

ACKNOWLEDGEMENT

This work is performed as part of the Partners for Advanced Transit and Highways (PATH) program, prepared under the sponsorship of the State of California; Business, Transportation and Housing Agency; Department of Transportation (CalTrans).

We would like to express our sincere thanks to S. Shladover of California PATH, M. Tomizuka and K. Hedrick of the University of California at Berkeley, J. Ackermann, W. Sienel and T. Bünte of DLR (Germany), K. Åström of Lund University (Sweden), and the anonymous reviewers for their insightful comments and suggestions.

REFERENCES

1. J.G. Bender, "An overview of systems studies of automated highway systems", IEEE Trans. on Vehicular Technology, vol. 40, no. 1, pp. 82–99, 1991.
2. S.E. Shladover, "Review of the state of development of advanced vehicle control systems (AVCS)", Vehicle System Dynamics, vol. 24, pp. 551–595, 1995.
3. P. Varaiya, "Smart cars on smart roads: Problems of control", IEEE Trans. on Automatic Control, vol. 38, pp. 195–207, 1993.
4. R.E. Fenton, G.C. Melocik, and K.W. Olson, "On the steering of automated vehicles: Theory and experiment", IEEE Trans. on Automatic Control, vol. 21, no. 3, pp. 306–315, 1976.

5. W. Darenberg, "Automatische Spurführung von Kraftfahrzeugen (in German)", Automobil-Industrie, pp. 155–159, 1987.
6. R.J. Mayhan and R.A. Bishel, "A two-frequency radar for vehicle automatic control", IEEE Trans. on Vehicular Technology, vol. 31, no. 1, 1982.
7. W. Zhang and R.E. Parsons, "An intelligent roadway reference system for vehicle lateral guidance/control", in Proc. American Control Conf., San Diego, CA, USA, 1990, pp. 281–286.
8. K.A. Ünyelioğlu, C. Hatipoğlu, and Ü. Özgüner, "Design and stability analysis of a lane following controller", IEEE Trans. on Control Systems Technology, to appear in 1996.
9. D. Margolis and Y. Yasui, "Automatic lateral guidance control system", US Patent no. 5390119, pp. 1–18, Feb. 14, 1995.
10. H. Peng, W.-B. Zhang, S.E. Shladover, M. Tomizuka, and A. Arai, "Magnetic-marker-based lane keeping: A robustness experimental study", in Proc. SAE Congress, SAE paper no. 930556, Detroit, MI, USA, 1993, pp. 127–132.
11. S. Patwardhan, M. Tomizuka, W.-B. Zhang, and P. Devlin, "Theory and experiments of tire blow-out effects and hazard reduction control for automated vehicle lateral control system", in Proc. Int. Symp. on Advanced Vehicle Control, Japan, 1994, pp. 426–431.
12. R.E. Fenton and R.J. Mayhan, "Automated highway studies at the Ohio State University – An overview", IEEE Trans. on Vehicular Technology, vol. 40, no. 1, pp. 100–113, 1991.
13. S.E. Shladover, "The California PATH program and its approach to vehicle-highway automation", in Proc. Intelligent Vehicles Symp., Detroit, 1992, pp. 347–352.
14. Lateral and Longitudinal Control Systems Working Group, "Overview of the R&D and test on automated highway systems (AHS)", in Intelligent Transport Systems, Tsukuba, Japan, November 1995.
15. H. Peng and M. Tomizuka, "Vehicle lateral control for highway automation", in Proc. American Control Conf., San Diego, CA, USA, 1990, pp. 788–794.
16. P. Riekert and T.E. Schunck, "Zur Fahrmechanik des gummibereiften Kraftfahrzeugs (in German)", Ingenieur Archiv, vol. 11, pp. 210–224, 1940.
17. J. Ackermann, A. Bartlett, D. Kaesbauer, W. Sienel, and R. Steinhauser, Robust control: Systems with uncertain physical parameters, Springer, London, 1993.